Modeling particulate removal in plate-plate and wire-plate electrostatic precipitators

S. Ramechecandane†1, Claudine Beghein‡, N. Eswari**
†System Engineer, FMC Technologies, NO-3601, Kongsberg, Norway
‡Associate Professor, Pole Sciences et Technologie, Universite de La Rochelle, La Rochelle 17000, France
**Cost Engineer, FMC Technologies, NO-3601, Kongsberg, Norway

ABSTRACT

The present study is concerned with the modeling of electrically charged particles in a model plate-plate and a single wire-plate electrostatic precipitator (ESP). The particle concentration distributions for both a plate-plate and a wire-plate ESP are calculated using a modified drift flux model. Numerical investigations are performed using the modified drift flux model for particle number concentration, in addition to the RNG k - ε model for the mean turbulent flow field and the Poisson equation for the electric field. The proposed model and the outlined methodology for coupling the flow field, electric field, charging kinetics and particle concentration is applied to two model precipitators that are truly representative of a wide class of commercialized ESPs. The present investigation is quite different from the earlier studies as it does not make assumptions like a homogeneous electric field or an infinite turbulent diffusivity. The electric field calculated is a strong function of position and controls the migration velocity of particles. Hence, the proposed model can be implemented in a flow solver to obtain a full-fledged solution for any kind of ESP with no limitations on the particle number concentration, as encountered in a Lagrangian approach. The effect of turbulent diffusivity on particle number concentration in a plate-plate ESP is investigated in detail and the results obtained are compared with available experimental data. Similarly, the effect of particle size/diameter and applied electric potential on the accumulative collection performance in the case of a wire-plate ESP is studied and the results obtained are compared with available numerical data. The numerical results obtained using the modified drift flux model for both the plate-plate and wire-plate ESP are in close agreement with available experimental and numerical data.

Keywords: Electrostatic precipitators, Drift flux model, Wire-plate ESP, Plate-plate ESP, RNG k -ε model

1. INTRODUCTION

Electrostatic precipitators have been commercialized in a wide range of industries and pulverized coal fired power plants since the beginning of this century. It is a device collecting particulate matter from stack emission for preventing air pollution. Industrial and power plant electrostatic precipitators consist of a series of grounded parallel plates through which stack emission/flue gas is passed. A series of equally spaced thin electrode wires at very high

[1]Corresponding Author; phone: +47 95446874; email: ramechecandan.somassoundirame@fmcti.com

potential (in the range of 40–80 kV) are located at the centerline of the flow channel. A very high potential at the thin wires that serve as discharge electrodes leads to a corona discharge. A corona is nothing but a current that develops from an electrode with a high potential in a neutral fluid like air, by ionizing that fluid to create plasma around the electrode. The ions generated due to the ionizing of the fluid pass the charge to the nearby areas of lower potential. The particles are ionized because of these ions that are generated from the electrode with a high potential. The dispersed ions leads to a secondary flow field that is totally dependent on the corona discharge. This secondary flow is normally referred to as electric wind, corona wind or ionic wind. Coronas may be positive or negative and is determined by the polarity of the voltage on the electrode. The particles in the flue gas/stack emission acquire an electric charge of the same polarity of that of the discharge electrode. Electrical discharge from the wire/discharge electrodes that are usually maintained at high negative potential produces gaseous ions by attachment of free electrons to gaseous molecules. The particles are charged by frequent collisions with the gaseous molecules.

Rigorous new regulations in dust emission by industries and coal fired power plants have led to an increase in the demand of efficient dust control devices. Electrostatic precipitators that are widely used in coal fired power plants, mining installations, metallurgical, waste incineration plants, cement and chemical industries are classified into single stage and double stage ESPs based on whether the particle charging and collection occur simultaneously. A vast majority of these ESPs ensures collection efficiency greater than 90%. The gas velocity within the ESP is usually in the range of 0.5–1.5 m/s, and the typical migration velocity of particles to the collector plate/collecting electrode lies between 0.02 to 0.15 m/s. The current density on the collection electrode is usually of the order of 0.1–1 mA/m^2. The pressure drop within a conventional ESP is not higher than 1–2 kPa, and the energy consumption lies within the range of 0.3–1.8 MW/1000 N m^3 [1]. Typically, the particles in stack emission/flue gases have a wide particle size distribution ranging between 50 to 100 μm down to the submicron range [2]. Particles larger than 3 μm in diameter and smaller than 0.1 μm can be effectively removed by an ESP. The minimum in the fractional collection efficiency of a conventional electrostatic precipitator (ESP) is observed in the 0.1 to 1 μm diameter range, where it is usually lower than 90 %. The low precipitation efficiency of the submicron/ultrafine particles is owing to the fact that charging these particles with a large number of units of elementary charges is quite difficult. The physics behind the charge density distribution in a wire–plate (single - stage ESP) is quite different from a plate - plate ESP (two - stage ESP). In a wire–plate ESP the particles are charged due to the ionic wind and hence acquire a charge based on the corona discharge from the wire electrodes whereas in the case of a plate–plate ESP the particles are pre-charged before entering the plate–plate ESP [3].

Though the Lagrangian approach to particle tracking still remains as the most reliable [4–5], the Eulerian approaches such as the drift flux model and mixture model can also yield reliable results with very little computational effort. The drift flux model can be modified based on the drift fluxes induced by external effects such as gravitational, drag, electrostatic and magnetic forces. The computational effort associated with a Lagrangian approach is quite extensive as the particle number concentration increases. The Lagrangian approach is suitable for very dilute flows where the particle number concentration is less. An extensive review of literature reveals that the vast majority of the modeling works on ESP are performed using the Lagrangian approach [6–9]. The availability of literature pertaining to the numerical modeling of ESP using the Eulerian approach is scarce, notable being the works of Leonard et al. [10,11]. A lot of assumptions were made in the works of

Leonard et al. [10,11] the convection diffusion equation is solved separately from the flow field with experimentally observed values of turbulent diffusivities (0.6, 1.2 and 30 cm^2/s). Such assumptions are quite common in a lot of earlier works on ESP. Modeling the turbulent dispersion coefficient is a crucial point in Eulerian models. Most authors of the earlier works use a constant value of the dispersion coefficient in the range of 1–50 cm^2/s [6, 10, 11]. Almost all of the earlier works on Lagrangian modeling of particle dispersion in an ESP were restricted to two dimensions as the particle tracking in a three dimensional space could be computationally expensive and pose a horrendous task.

A major issue that stimulates research activity in the field of electrostatic precipitation is submicrometer particulate removal. Not many of the previous studies have considered the ultrafine/submicron particles (<0.1 μm) or the accumulation mode particles (0.1 to 2.5 μm) in the modeling of an ESP. The major reason for ignoring the effects of particles smaller than 1 μm is that they constitute only 1 % of the total mass. Though the contribution of such smaller sized particles to the mass is less these particles occupies 99 % of the number concentration. Hence, a detailed investigation on the dispersion and deposition of such particles is very important as they are major threat to the environment. The fraction of toxic metals is significantly higher in submicrometer particles, and it is independent of particle size.

The present paper considers two cases of a single-stage and two-stage ESP that are truly representative of a wide class of ESPs in common use. A modified drift flux model is used to calculate the particle number concentration in an inhomogeneous electric field for the two model ESPs (wire-plate ESP and plate-plate ESP). The objective of the present study is to propose a methodology to simulate the dispersion and deposition of particles that are subjected to an inhomogeneous electric field within an ESP. Special attention is bestowed on the modeling of ultrafine particulate removal as it poses a serious threat to the environment.

2. MATHEMATICAL FORMULATION

In this section the modified drift flux model proposed for the analysis is developed. The development of the model is carried out in a sequential manner. In the first subsection 2.1 on flow field, the continuity and the momentum equations that need to be solved for the present analysis are explained in detail. The subsection 2.2 on drift flux model explains the widely accepted drift flux model with a means of modeling the Brownian diffusivity. The subsection 2.3 on the modeling of electric field gives a list of equations that are to be solved to obtain a complete solution for an inhomogeneous electric field. The subsection 2.4 on particle charging kinetics attempts to explain the number of units of charge that a particle might acquire when exposed to an electric field. Finally, the modifications that are made for the existing drift flux model is explained in subsection 2.5 with the assumptions listed below:

(i) The particles are assumed to be spherical in shape.
(ii) The interactions between particles like collisions and coagulation/agglomeration can be neglected.
(iii) There exists no bounce-off or re-entrainment of the particles once they reach the collecting wall. i.e., the collecting walls are assumed to be perfect absorbers.

2.1 FLOW FIELD

Using Reynolds averaging, the continuity and momentum equations in Cartesian coordinates are:

$$\frac{\partial \rho}{\partial t} + \frac{\partial}{\partial x_i}(\rho u_i) = 0 \tag{1}$$

$$\frac{\partial}{\partial t}(\rho u_i)+\frac{\partial}{\partial x_j}(\rho u_i u_j)=-\frac{\partial \rho}{\partial x_i}+\frac{\partial}{\partial x_j}\left[\mu\left(\frac{\partial u_i}{\partial x_j}+\frac{\partial u_j}{\partial x_i}-\frac{2}{3}\delta_{ij}\frac{\partial u_i}{\partial x_j}\right)\right]+\frac{\partial}{\partial x_j}(-\rho u_i' u_j') \quad (2)$$

The Reynolds stresses $\rho u_i' u_j'$ in the eqn. 2 must be modeled in order to close the equation. A common method employs the Boussinesq hypothesis to relate the Reynolds stresses to the mean velocity gradients

$$-\overline{\rho u_i' u_j'}=\mu\left(\frac{\partial u_i}{\partial x_j}+\frac{\partial u_j}{\partial x_i}\right)--\frac{2}{3}\delta_{ij}\left(\mu_t\frac{\partial u_i}{\partial x_i}+\rho k\right) \quad (3)$$

The Boussinesq hypothesis is used in many models like the Spalart-Allmaras model, the *k*- ε models, and the *k*- ω models. The advantage of this approach is the relatively low computational cost associated with the computation of the turbulent viscosity (μ_t) In the case of the RNG *k*- ε model, two additional transport equations (for the turbulence kinetic energy *k*, and the turbulence dissipation rate ε) are solved, and μ_t is computed as a function of *k* and ε.

$$\frac{\partial}{\partial t}(\rho k)+\frac{\partial}{\partial x_j}(\rho k u_i)=\frac{\partial}{\partial x_j}\left[\alpha_k\left(\mu_{eff}\frac{\partial k}{\partial x_j}\right)\right]+G_k-\rho\varepsilon \quad (4)$$

$$\frac{\partial}{\partial t}(\rho \varepsilon)+\frac{\partial}{\partial x_j}(\rho \varepsilon u_i)=\frac{\partial}{\partial x_j}\left[\alpha_s\left(\mu_{eff}\frac{\partial \varepsilon}{\partial x_j}\right)\right]+C_{1s}G_k\frac{\varepsilon}{k}-C_{2s}\rho\frac{\varepsilon^2}{k}-R_s \quad (5)$$

$$\mu_t=\rho C_\mu\frac{k^2}{\varepsilon} \quad (6)$$

The disadvantage of the Boussinesq hypothesis as presented is that it assumes μ_t is an isotropic scalar quantity, which is not strictly true. The major parameters that differentiate RNG k–ε model from the standard k–ε model are the constants involved in the equations (4) and (5) and the term R_s that is present in the right hand side of eqn (5) and is given by.

$$R_s=\frac{C_\mu\rho\eta^3\left(1-\frac{\eta}{\eta_0}\right)\varepsilon^2}{1+\beta\eta^3}\frac{\varepsilon^2}{k} \quad (7)$$

The values of constants involved in eqns (4), (5) and (6) are given in table. 1

The term G_k representing the production of turbulent kinetic energy is modeled as

$$G_k=-\overline{\rho u_i' u_j'}\left(\frac{\partial u_j}{\partial x_i}\right) \quad (8)$$

In a wire-plate ESP the ionic wind interacts with the flow field of the ESP and produces a highly complex fluid dynamic flow field [2,5]. In order to obtain the flow field of a wire-plate ESP the following momentum equations needs to be solved.

Table 1: Constants involved in the RNG k–ε model

C_μ	C_{1s}	C_{2s}	α_k	α_s	η_0	β
0.0845	1.42	1.68	1.39	1.39	4.38	0.012

$$\frac{\partial}{\partial t}(\rho u_i)+\frac{\partial}{\partial x_j}(\rho u_i u_j)=-\frac{\partial p}{\partial x_i}+\frac{\partial}{\partial x_j}\left[\mu\left(\frac{\partial u_i}{\partial x_j}+\frac{\partial u_j}{\partial x_i}-\frac{2}{3}\delta_{ij}\frac{\partial u_i}{\partial x_j}\right)\right]+\frac{\partial}{\partial x_j}(-\rho u_i' u_j')+\rho_{el,I}\mathrm{E_j} \quad (9)$$

The continuity eqn (1) and the modified momentum equation (9) with the RNG k–ε model (Eqns. 4-8) for the mean turbulent flow field are solved using an opensource CFD code–OpenFOAM–version 1.5.

2.2 DIFFUSION MODEL / DRIFT FLUX MODEL

The Eulerian approach is used for gaseous pollutants and ultrafine particles cum accumulation mode particles, which are treated as transferable scalars. The convection-diffusion equation for species transport is given as [2, 5]

$$\frac{\partial \mathrm{C}^{\alpha}}{\partial \mathrm{t}}+\mathrm{u_j}\frac{\partial \mathrm{C}^{\alpha}}{\partial \mathrm{x_j}}=\frac{\partial}{\partial \mathrm{x_j}}\left(\left(\mathrm{D}^{\alpha}+\frac{\nu_t}{\mathrm{Sc}_t^{\alpha}}\right)\frac{\partial \mathrm{C}^{\alpha}}{\partial \mathrm{x_j}}\right) \quad (10)$$

Where, C^{α} is the concentration of the pollutant species "α" and D^{α} is its diffusivity, υ_t is the turbulent eddy viscosity and $Sc_t^{\alpha} = \nu_t/D_t^{\alpha}$ is turbulence Schmidt number, with D_t^{α} being the turbulent diffusivity of species α. The concentration C^{α} of the pollutant species α can be expressed on mass (kg/m^3) or number basis (#/ m^3). The Neumann boundary condition, $\frac{\partial \mathrm{C}^{\alpha}}{\partial \mathrm{n}}=0$ is applied at the walls. For modelling ultrafine particulate materials, the particle diffusivity is given as [12]

$$\mathrm{D}^{\alpha}=\frac{\mathrm{k}_{\beta}\mathrm{TC_c}}{3\pi\mu\mathrm{d_p}} \quad (11)$$

The particle diffusion coefficient D^{α} accounts for the Brownian motion of the particles. Here, d_p is the diameter of the particle, $k_\beta = 1.38 \times 10^{-23}$J/K is the Boltzmann constant, T is the absolute temperature and μ the dynamic viscosity of air. C_c is the Cunningham correction factor also referred to as the slip correction factor or the Cunningham slip factor, it is given as,

$$C_c=1+\frac{2\lambda}{\mathrm{d_p}}\left[1.257+0.4e^{-1.1\mathrm{d_p}/2\lambda}\right] \quad (12)$$

Here, λ denotes the molecular mean free path in the gas. For atmospheric air, under standard temperature and pressure condition (STP) λ is equal to 66nm. For large particles, the diffusion coefficient for Brownian motion assumes negligible small values. Considering a particle size of 1 micron and a fluid dynamic viscosity of 1.8×10^{-5} kg m/s once could estimate from Eq. (11) that the value of D^{α} is 2.5×10^{-11} m^2/s. The effect of turbulent diffusivity is more pronounced in micro sized particles and hence the diffusion coefficient for Brownian motion is usually ignored. Whereas, in case of sub-micron sized particles or nano-particles the Brownian motion is a very important phenomenon and the effect of Brownian diffusivity cannot be ignored.

When an external force like gravity, electrostatic or magnetic acts on the particles, the diffusion equation can be modified and rewritten as

$$\frac{\partial \mathrm{C}^{\alpha}}{\partial \mathrm{t}}+(\mathrm{u_j}+\mathrm{u_j^t})\frac{\partial \mathrm{C}^{\alpha}}{\partial \mathrm{x_j}}=\frac{\partial}{\partial \mathrm{x_j}}\left(\left(\mathrm{D}^{\alpha}+\frac{\nu_t}{\mathrm{Sc}_t^{\alpha}}\right)\frac{\partial \mathrm{C}^{\alpha}}{\partial \mathrm{x_j}}\right) \quad (13)$$

Where u_j^t is normally referred to as the terminal velocity or the drift velocity of the particles that are subjected to the external force field. The modified diffusion Eq. (13) is generally referred to as the drift flux model.

2.3 SIMULATION OF ELECTRIC FIELD

In the present study a numerical solution of the electric field is obtained by solving the Poisson equation and the equation for charge continuity.

The electric field is given as,

$$\vec{E} = -\overrightarrow{grad}\,\varphi \tag{14}$$

Where φ is the applied voltage, and is obtained by solving the Poisson equation

$$\Delta\varphi = -\frac{\rho_{el,I} + \rho_{el,p}}{\varepsilon_0} \tag{15}$$

Where, $\varepsilon_0 = 8.859 \times 10^{-12}\ A\ sV^{-1}m^{-1}$ is the dielectric permittivity of air; $\rho_{el,I}$ and $\rho_{el,p}$ are the ionic and particulate space charge respectively. The continuity equation for the ionic space charge neglecting the effects of mean fluid flow convection and diffusion is given by [2, 5]

$$\text{div}\ \overrightarrow{J_{el,I}} = 0 \tag{16}$$

$$\overrightarrow{J_{el,I}} = \rho_{el,I}\, b_I \vec{E} \tag{17}$$

In the present investigation, the particles are assumed to be electrically charged even before entering the electric field and hence acquire an electrical migration velocity purely based on the electric field and the number of charges already on the particles. The total number of charges on a single particle is calculated as shown in the ensuing section on charging kinetics.

Where, $b_I = 2 \times 10^{-4} m^2 V^{-1} s^{-1}$ is the ionic mobility.

The contribution of ions may be neglected in the case of a plate-plate electrostatic two stage precipitator as a corona discharge does not occur in it. For a corona discharge to occur the electrodes must be of different shapes in particular the discharge electrode must be curved. So, in the case of a plate-plate ESP the space charge density is equal to the particle number concentration C_0 at the inlet multiplied by the charge q_p of a single particle for monodispersed particles.

$$\rho_{el,p} = q_p\, C^{\alpha} \tag{18}$$

Eqs. (15) and (16) form a set of partial differential equations that are to be solved for computing the potential field and thereby, the electric field with the charge density distribution for a wire–plate electrostatic precipitator. In the case of a plate-plate electrostatic precipitator the Poisson equation (15) is solved by computing the particulate space charge using eqn. (18).

2.4 PARTICLE CHARGING

The number of units of charge on a particle needs to be calculated by taking into account the various charging mechanisms like the static electrification, tribo-electrification, Boltzmann charge distribution, the diffusion charging and the field charging mechanisms. One can

decide from existing literature [4] that the diffusion and field charging mechanism is more apt for micro-sized particles. In the presence of an electric field, the particles acquire charge by frequent collisions with the unipolar ions. This phenomenon is normally referred to as field charging. The effect of field charging is quite significant for particles that are larger than 1μm in size and increases with the square of the particle size. After sufficient time at a given charging condition, the maximum saturation number of charges "n_{field}", acquired by the particles is given by,

$$n_{field} = \left(\frac{3\varepsilon_0}{\varepsilon_0 + 2} \right) \left(\frac{E\, \mathrm{d_p^2}}{4e} \right) \tag{19}$$

Where, E is the magnitude of the Electric field, $\varepsilon_0 = 8.859 \times 10^{-12}\ A\ s\ V^{-1}m^{-1}$ is the dielectric permittivity, $e = 1.6 \times 10^{-19}$ C is the electronic unit charge.

Diffusion charging is mainly due to the random collisions of unipolar ions and particles due to Brownian motion. The modelling of the Brownian motion is very important in tracking the particle trajectory. For particles less than 1μm in size, diffusion charging is the main charging mechanism. Hence, for nanoparticles the contribution of the diffusion charging mechanism is quite significant as compared to that of field charging and Boltzmann charge distribution. The approximate number of charges acquired by a particle of diameter $\mathrm{d_p}$ is given by,

$$n_{diffusion} = \left(\frac{\mathrm{d_p k_\beta T}}{2e^2} \right) ln \left(1 + \frac{\pi \mathrm{d_p} \bar{c}_l \mathrm{e^2 N_i t}}{2\mathrm{k_\beta T}} \right) \tag{20}$$

Where, $\mathrm{k_\beta} = 1.38 \times 10^{-16}$ erg $\mathrm{K^{-1}}$ is the Boltzmann constant, T is the temperature of the gas and equals to 288 K, $e = 1.6 \times 10^{-19}$ C is the electronic unit charge, t stands for time, $\bar{c}_l = 2.4 \times 10^{24}$ cm $\mathrm{s^{-1}}$ is the mean thermal speed of ions and $\mathrm{N_t}$ is the ions concentration.

The total number of charges that a single particle can acquire by both field charging and diffusion charging mechanisms is given by,

$$q_p = \left(n_{field} + n_{diffusion} \right) e \tag{21}$$

Where, e is the electronic unit charge. The particular space charging phenomenon is totally dependent on the estimation of the total number of charges that a particle can acquire.

2.5 MODIFIED DRIFT FLUX MODEL

The modified drift flux model to account for the drift flux caused by the inhomogeneous electric field is given by [2, 5]

$$\frac{\partial \mathrm{C}^\alpha}{\partial \mathrm{t}} + (\mathrm{u_j} + \mu_\mathrm{p} \mathrm{E_j}) \frac{\partial \mathrm{C}^\alpha}{\partial \mathrm{x_j}} + \frac{\rho_{el,I} + \rho_{el,p}}{\varepsilon_0} \mu_\mathrm{p} \mathrm{C}^\alpha = \frac{\partial}{\partial \mathrm{x_j}} \left(\left(\mathrm{D}^\alpha + \frac{\nu_\mathrm{t}}{\mathrm{Sc_t^\alpha}} \right) \frac{\partial \mathrm{C}^\alpha}{\partial \mathrm{x_j}} \right) \tag{22}$$

Where, μ_p the dielectric particle mobility or the electrical mobility of a particle is given by

$$\mu_\mathrm{p} = \frac{q_p \mathrm{C_e}}{3\pi\mu \mathrm{d_p}} \tag{23}$$

The modified drift flux model given by Eq. (22) is solved to obtain the normalized concentration for various particle sizes/diameters. In equation 22 the term $\mu_\mathrm{p}\mathrm{E_j}$ is normally referred to as the electrical migration velocity given by equating the Coulomb force to the Stokes drag. The electrical migration velocity w_e is given by,

$$w_e = \frac{q_p C_c E}{3\pi\mu d_p} \tag{24}$$

The numerical analysis employed to solve the present problem is based on the finite volume formulation with the central difference scheme for the diffusion terms and the upwind weighted scheme for the convection terms to eliminate the false diffusion. Euler implicit scheme is employed for the temporal discretization and the spatial discretizations are second order accurate.

3. RESULTS AND DISCUSSION

3.1 PLATE-PLATE ESP

The geometry of the plate-plate ESP considered for the present investigation is shown in Fig.1. The precipitator modeled closely resembles the collection stage of a two-stage ESP. The particles that are precharged in a precharger or the first stage of the ESP enters the collection stage totally charged. The precharged particles enter the collection stage with uniform concentration and they traverse at the exhaust/flue gas velocity. Inlet velocities of gas and particles are 3.0 m/s and the turbulence intensity of the main flow is less than 0.3 %. The precipitator has a plate-plate spacing of 0.05 m and an overall length of 0.75 m. The lower plate acts as a discharge electrode (high voltage electrode) and the upper grounded plate serves as a collecting electrode. The flue gas/stack emission along with the monodispersed precharged particles enters the collection stage of a plate-plate ESP. The particles move towards the collecting grounded electrode with a migration velocity w_e usually referred to as the electrical migration velocity caused by the Coulomb force.

The geometry considered for the present investigation on plate-plate electrostatic precipitator is similar to the model precipitator of Leonard et al [10]. The particle number density at the inlet of the plate-plate ESP is taken as 5×10^8 particles/m^3. The experimental data of Leonard et al serves as the base for this investigation on plate-plate ESP. A grid independence study is carried out for the geometry considered and an optimal

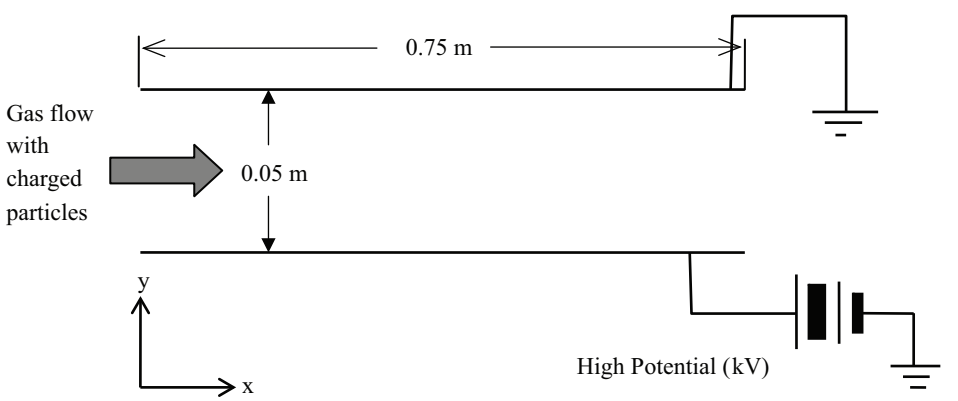

Figure 1: Schematic geometry of the plate-plate electrostatic precipitator

Table 2: Boundary conditions for the plate-plate ESP

	x–velocity (m/s)	y–velocity (m/s)	Electric potential (V)	Particle fate
Inlet	3.0	0	$\frac{\partial \varphi}{\partial x} = 0$	escape
Outlet	constant static pressure	$\frac{\partial p}{\partial x} = 0$	$\frac{\partial \varphi}{\partial x} = 0$	escape
Collecting Plate	no slip	no slip	$\varphi = 0$	trap
Discharge plate	no slip	no slip	6800	reflect

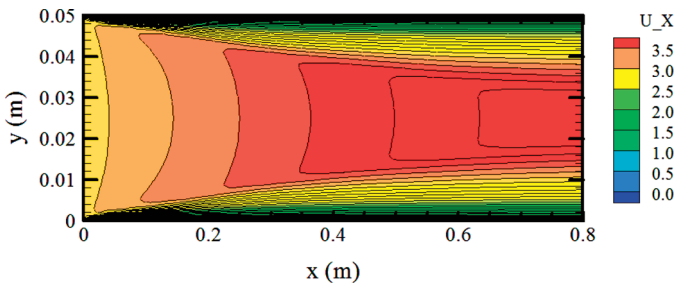

Figure 2: Contours of x-velocity (m s^{-1}) for the plate-plate electrostatic precipitator of Leonard et al [10]

grid size of 200000 hexahedral elements is considered for the numerical analysis. The grid near the walls is sufficiently fine enough to ensure a y^+ value less than 1 at the walls. The boundary conditions that are used for the present investigation are shown in Table. 2. The number of grids along the vertical direction is set as 40 with a geometric progression of 1.1. A time step of 0.001 s has been used to achieve a Courant Frederick Lewy number (CFL) value less than 1. An explicit scheme has been used for time marching. The convergence criteria/residuals for continuity, momentum and turbulent equations are set as 10^{-06}. The duration of flow has been set high enough for the flow to reach steady state. The simulations take approximately 48 hours for convergence in a desktop computer with 4 GB ram.

The contours of x-velocity are shown in Fig. 2. Figs.3 and 4 shows the contours of normalized electrical potential distribution and the normalized concentration for an applied electrical potential of 6800 V at the discharge electrode. The modified drift flux model is used for calculating the particle number concentration at various locations in the plate-plate ESP. To verify the accuracy of the numerical results obtained using the present model the particle number concentration at three different locations (0.05 m, 0.025 m and 0.045 m) are compared with the experimental data of Leonard et al [10]. The turbulent diffusivities are assumed to be a constant as furnished by the experimental data. For two

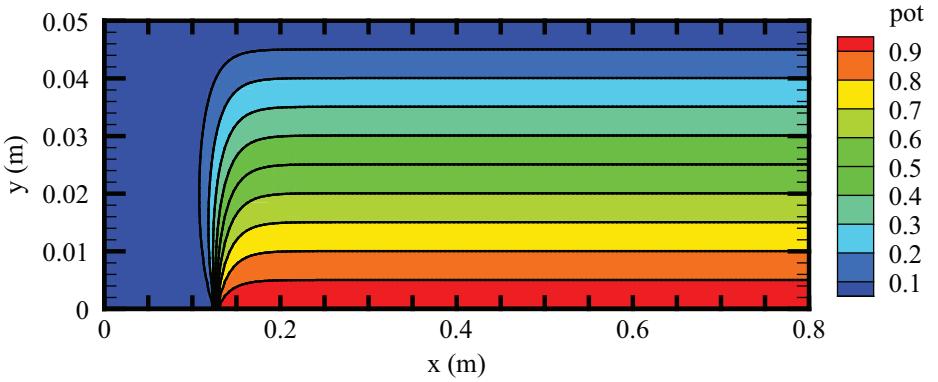

Figure 3: Contours of normalized electrical potential distribution for an applied electrical potential of 6800 V at the discharge electrode

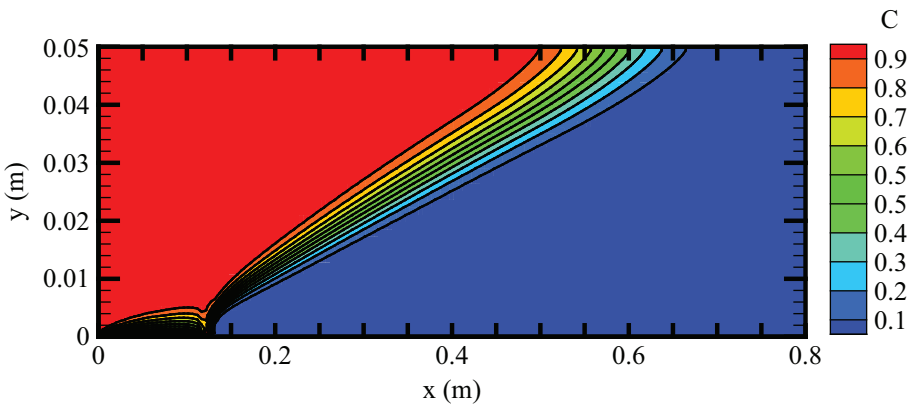

Figure 4: Contours of normalized concentration distribution for a turbulent diffusivity of 1.2 cm^2/s

different turbulent diffusivities 1.2 cm^2/s and 0.6 cm^2/s, the numerical results obtained are plotted in Figs. 5 (a) and 5 (b). The normalized concentration profiles for various values of immigration velocities corresponding to the two turbulent diffusivities (1.2 cm^2/s and 0.6 cm^2/s) are presented in Figs. 6(a) and 6(b). The results obtained using the modified drift flux model shows good agreement with the available experimental data. From figs. 5(a), 5(b), 6(a) and 6(b) it is clearly evident that the turbulent diffusivity has a great influence on the collection efficiency of a plate-plate electrostatic precipitator. The slight deviation between the numerical results obtained from the experimental data can be attributed to the inhomogeneous electric field. The electrical field strength is assumed to be homogeneous, constant in many previous investigations on ESPs [3,4,10] whereas in the present study the electric field is computed by numerically solving the Poisson equation.

3.2 WIRE-PLATE ESP

A schematic representation of the model wire-plate ESP considered for the present investigation is shown in Fig. 7. The wire-plate ESP consists of a single wire located

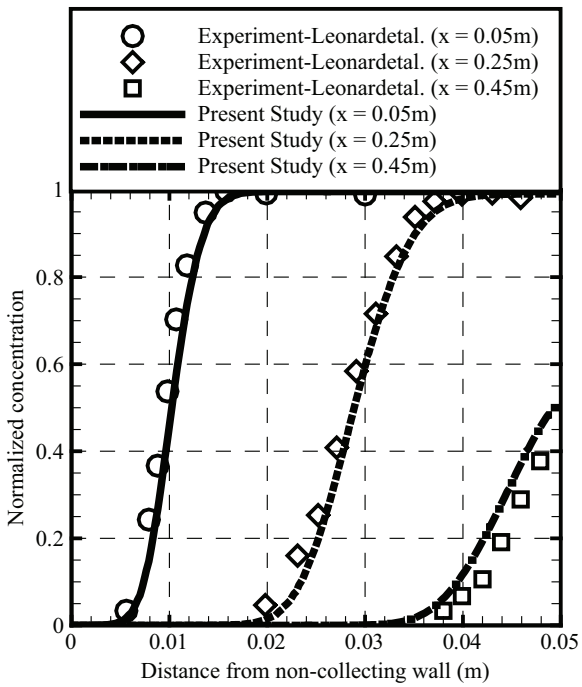

Figure 5: (a) Concentration distribution at three different locations along the flow (0.05 m, 0.25 m and 0.45 m) for a turbulent diffusivity of 1.2 cm^2/s ((Particle concentration profiles u = 3.0 m/s; wy = 0.3 m/s; D = 1.2×10^{-4} m^2/s)

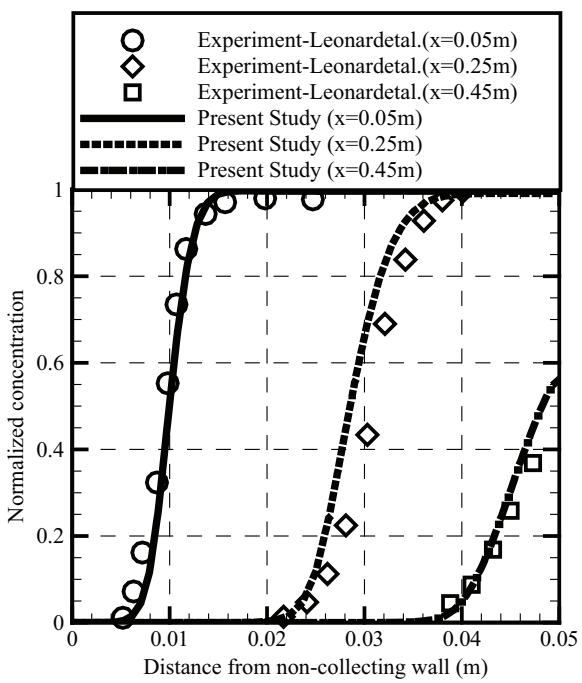

Figure 5: (b) Concentration distribution at three different locations along the flow (0.05 m, 0.25 m and 0.45 m) for a turbulent diffusivity of 0.6 cm^2/s (Particle concentration profiles u = 3.0 m/s; wy = 0.3 m/s; D = 0.6×10^{-4} m^2/s)

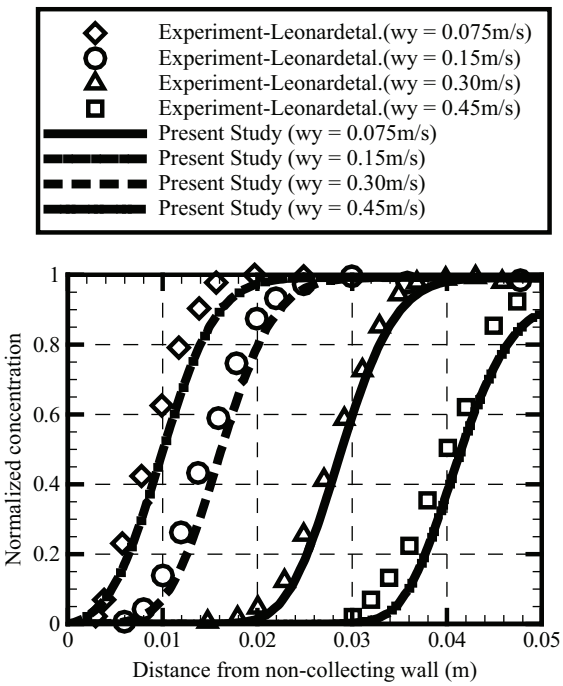

Figure 6: (a) Concentration distribution at three different locations along the flow (0.05 m, 0.25 m and 0.45 m) for various particle immigration velocities corresponding to a turbulent diffusivity of 1.2 cm^2/s (Particle concentration profiles; u = 3.0 m/s; x = 0.25 m; D = 1.2×10^{-4} m^2/s)

between two parallel collector plates. The wire to plate spacing is 0.1 m. The wire/discharge electrode is 5 mm in diameter and is located at 0.075 m from the inlet. Owing to symmetry just one half of the geometry is considered for the numerical analysis. The collecting plate and the discharge wire are impermeable walls with no slip boundary conditions. The boundary to the left is the inlet through which the gas with the dispersed particles enters and the boundary to the far right is the outlet. The gas with the particles loaded enters the inlet with a velocity of 1 m/s. Inlet turbulence intensity is taken as 5 % of the inlet velocity. The particles are assumed to be mono-dispersed and the numerical investigations are carried out for three particle sizes (0.1 μm, 1 μm and 10 μm). A finite volume grid with 240 × 120 × 1 cells is employed for the present investigation. The computational domain is split into a number of blocks to generate a block-structured mesh of hexahedral elements. The part of the computational mesh close to the wire is shown in Fig.8. The grid generated for the present investigation is sufficiently fine enough to ensure a y^+ value less than1 near the walls. The boundary conditions for the present investigation on wire-plate ESP are given in table. 3.

To validate the electric field obtained by the numerical simulation, the computational results are compared with the often-quoted experimental works of Penney and Matick [13]. The electric potential and the charge density distribution are computed for the precipitator geometry of Penney and Matick [13] with the wire diameter of 2 mm and an applied voltage of 46.2 kV. The electric potential distribution along a line from the wire electrode to the

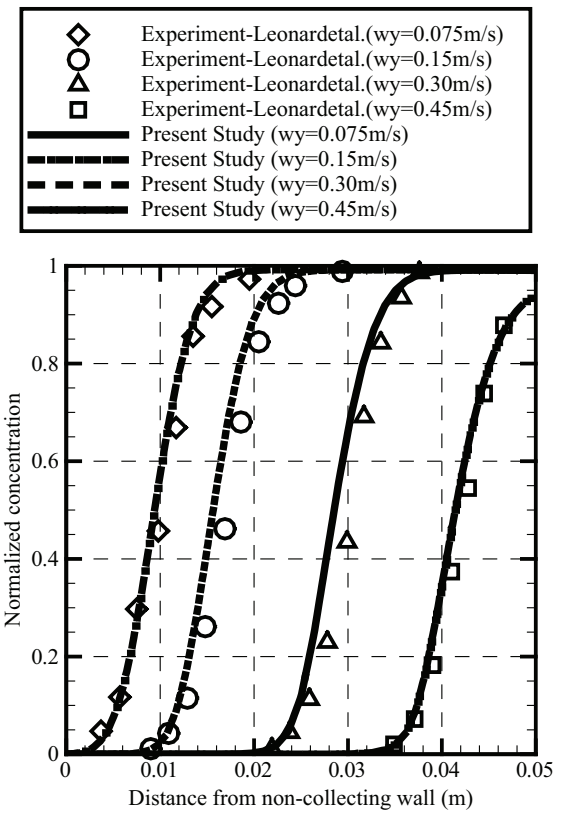

Figure 6: (b) Concentration distribution at three different locations along the flow (0.05 m, 0.25 m and 0.45 m) for various particle immigration velocities corresponding to a turbulent diffusivity of 0.6 cm^2/s (Particle concentration profiles; u = 3.0 m/s; x = 0.25 m; D = 0.6×10^{-4} m^2/s)

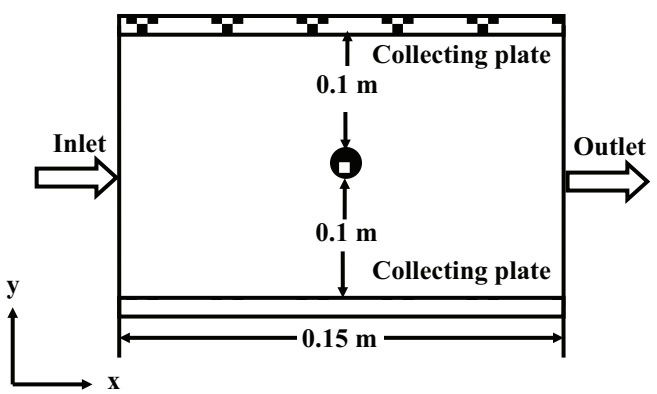

Figure 7: Model configuration for the wire-plate electrostatic precipitator (not to scale)

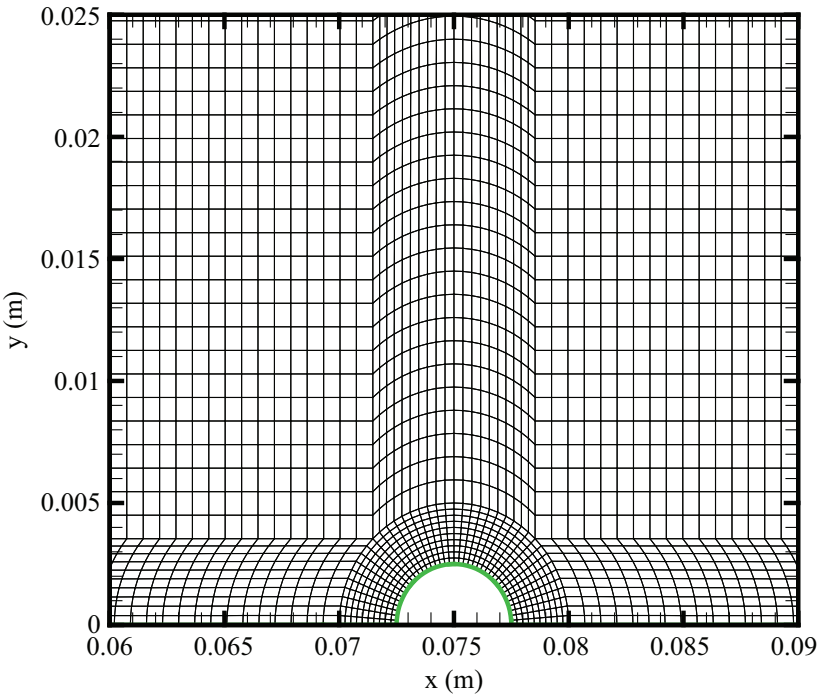

Figure 8: Computational mesh near the wire

Table 3: Boundary conditions for the wire-plate ESP

	x–velocity (m/s)	**y–velocity (m/s)**	**Electric potential (kV)**	**Ion charge density**	**Particle fate**
Inlet	1.0	0	$\frac{\partial \varphi}{\partial x} = 0$	$\frac{\partial \rho_{el,i}}{\partial x} = 0$	escape
Outlet	constant static pressure	$\frac{\partial p}{\partial x} = 0$	$\frac{\partial \varphi}{\partial x} = 0$	$\frac{\partial \rho_{el,i}}{\partial x} = 0$	escape
Collecting Plate	no slip	no slip	$\varphi = 0$	$\frac{\partial \rho_{el,i}}{\partial x} = 0$	trap
Discharge Wire	no slip	no slip	60, 70, 80	Peek's law	reflect

collector plate is plotted in Fig. 9 and the corresponding charge density distribution from the present study is shown in Fig. 10. The numerical results obtained using the present numerical simulation for the bench mark case of Penney and Matick shows a good agreement with the experimental data.

The contours of x-velocity component, turbulent kinetic energy, turbulent dissipation rate and the pressure are presented in Fig. 11. In Fig. 11 the region close to the discharge wire

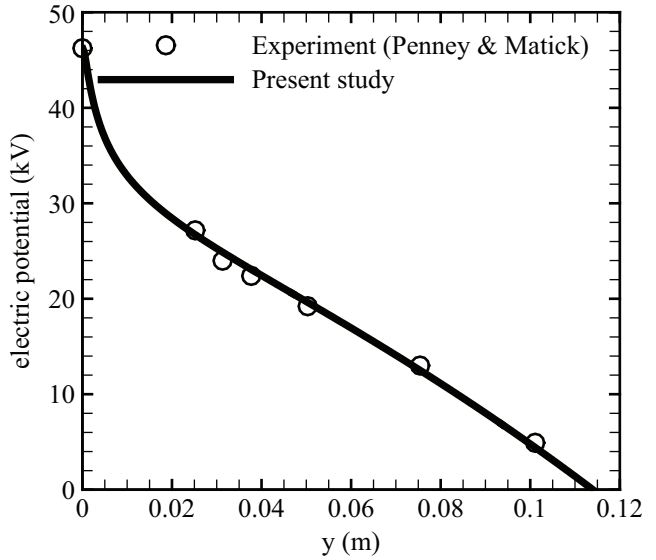

Figure 9: Electric potential distribution along a line from the wire electrode (discharge electrode) to the collector plate (collector electrode)

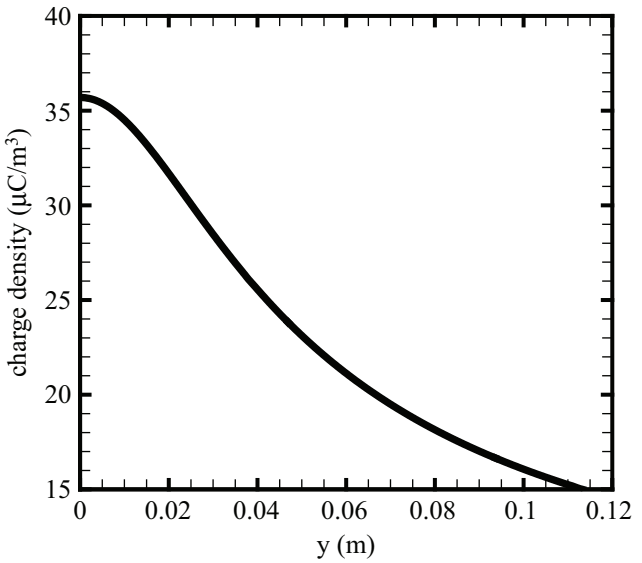

Figure 10: Charge density distribution along a line from the wire electrode (discharge electrode) to the collector plate (collector electrode)–Results from present study

electrode is enlarged to provide a closer view of the flow field. The contours of the electric field strength, electric potential distribution and the spatial charge density distribution are shown in Fig. 12, for an applied voltage of 70 kV. The electric potential distribution and the spatial charge density distribution are non-dimensionalized to obtain a comparison with the

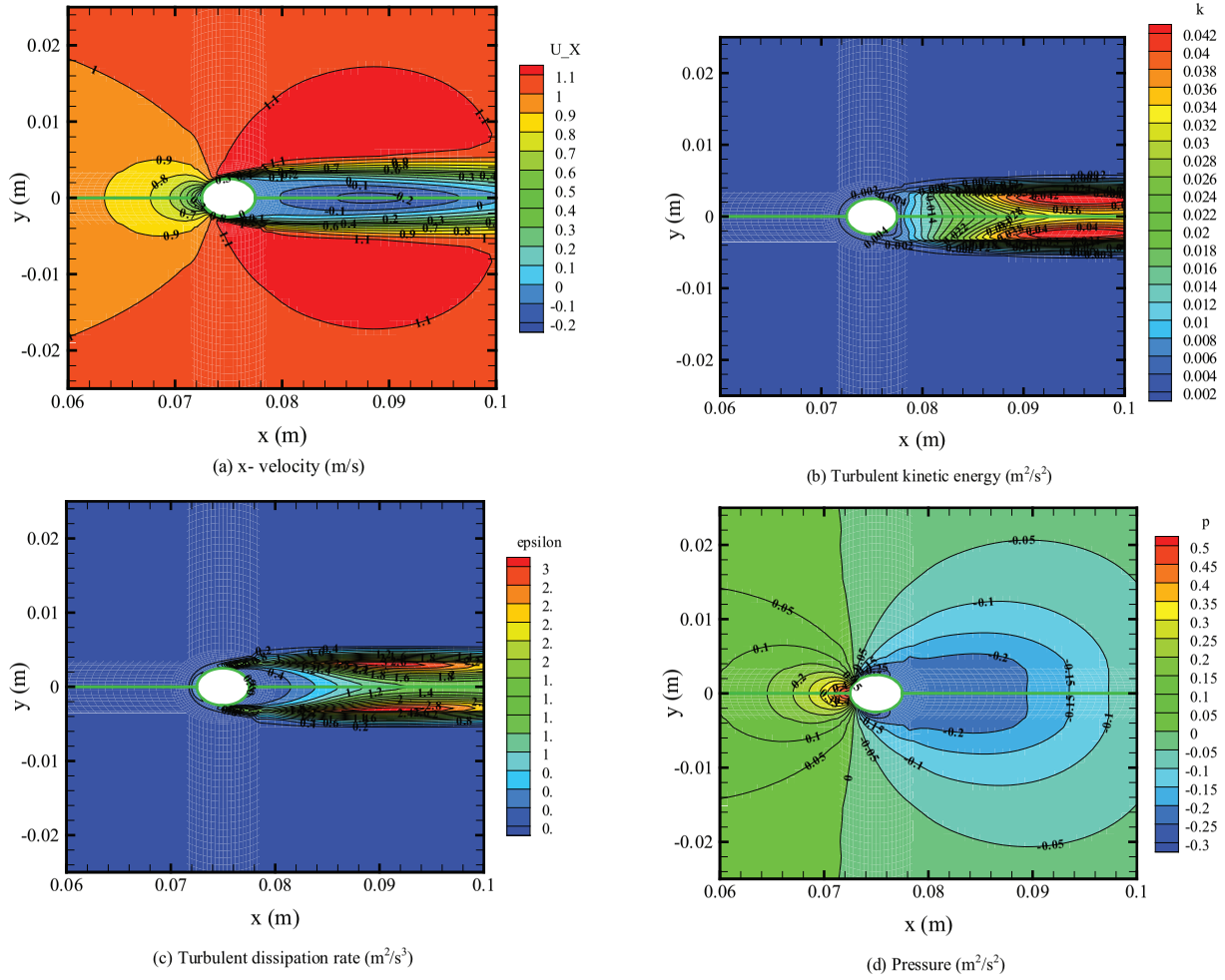

Figure 11: Contours of (a) x-velocity (m/s), (b) Turbulent kinetic energy (m^2/s^2), (c) Turbulent dissipation rate (m^2/s^3), (d) Pressure(m^2/s^2)

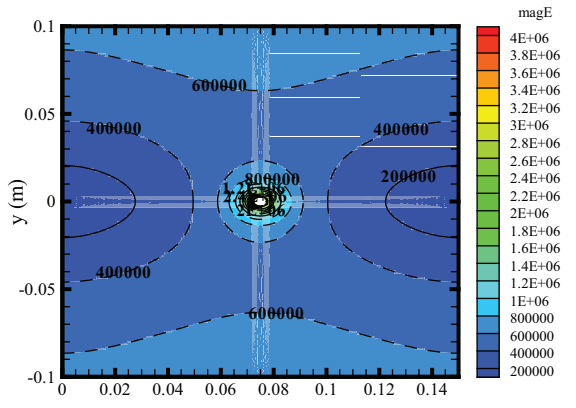

(a) Electric field magnitude (V/m)

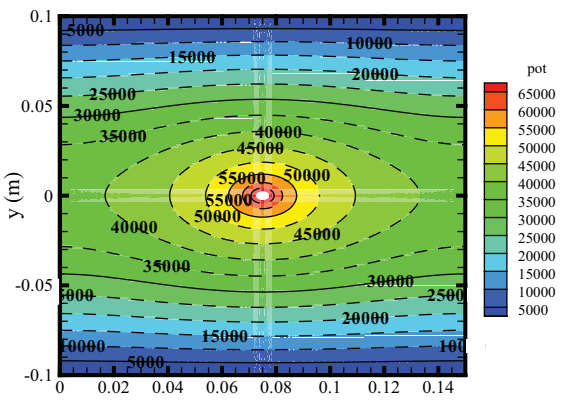

(b) Electric potential (V)

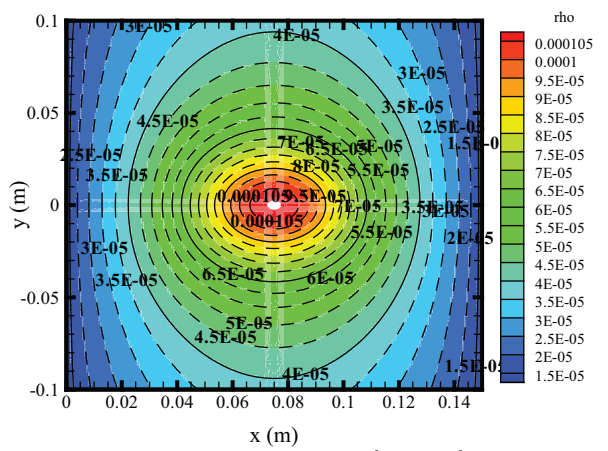

(c) Spatial charge density (As/m^3 or C/ m^3)

Figure 12: Contours of (a) Electric field magnitude (V/m), (b) Electric potential (V), (c) Spatial charge density (As/m^3 or C/ m^3)

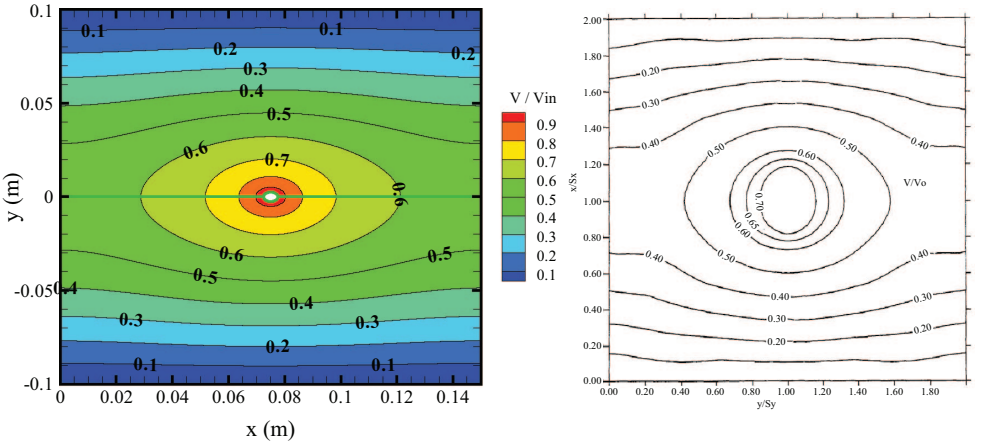

(a) Normalized electric potential – Present study (b) Normalized electric potential – Lami et al [14]

Figure 13: Normalized electric potential distribution (a) Present Study (b) Lami et al [14]

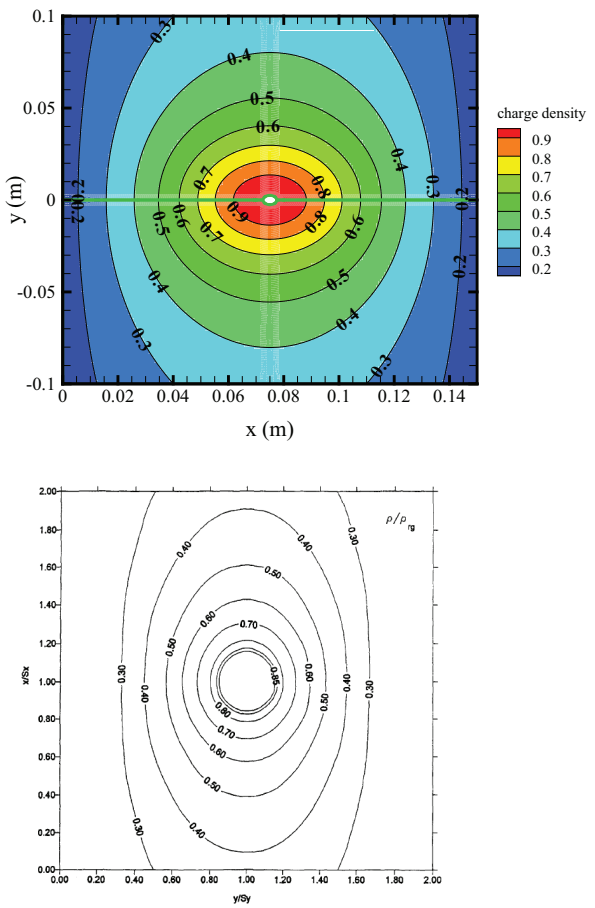

Figure 14: Normalized spatial charge density distribution (a) Present Study (b) Lami et al [14]

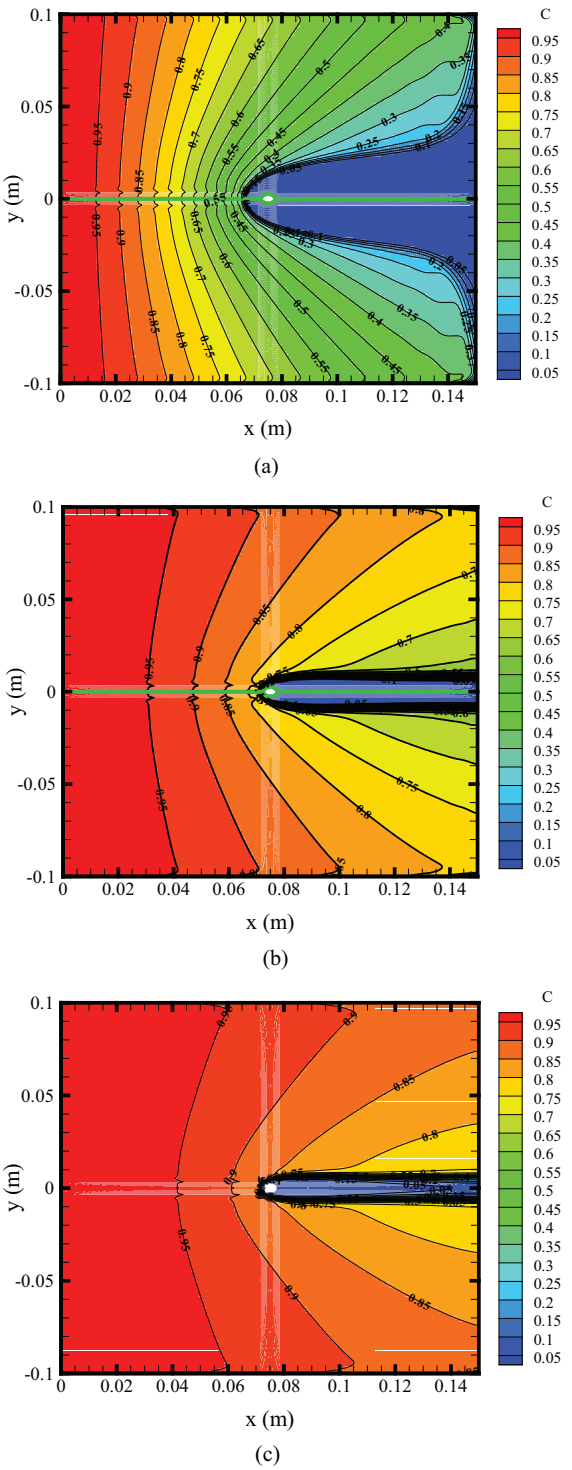

Figure 15: Normalized concentration distribution for a particle size of (a) 10 μm, (b) 1 μm, (c) 0.1 μm (applied voltage at wire 70 kV for an inlet velocity of 1 m/s)

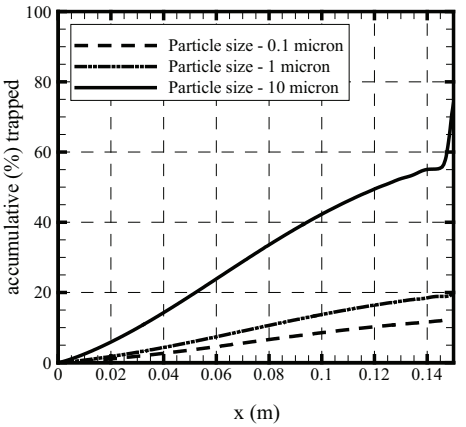

(a) Applied Voltage - 60 kV (inlet velocity – 1m/s)

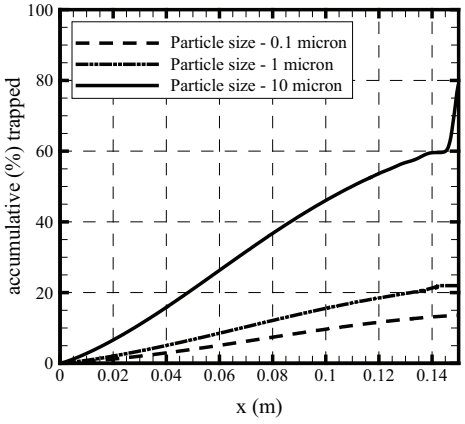

(b) Applied Voltage - 70 kV (inlet velocity – 1m/s)

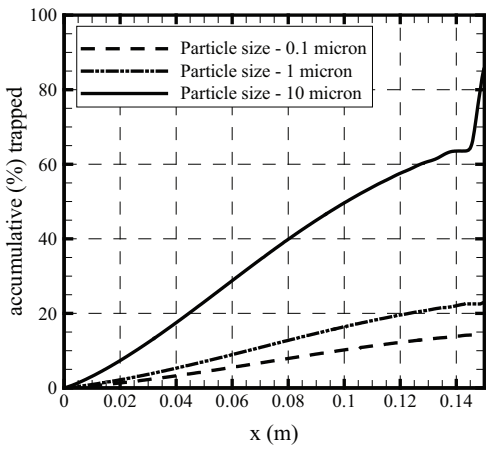

(c) Applied Voltage - 80 kV (inlet velocity – 1m/s)

Figure 16: Accumulative collection performance for different particle sizes (0.1 μm, 1 μm and 10 μm)

results of Lami et al [14]. The obtained results compare quite well with those of Lami et al [14] and are shown in Figs. 13 and 14. Fig. 15 shows the normalized concentration distribution for a particle size of 10 μm, 1 μm and 0.1 μm respectively, when the applied voltage at the wire discharge electrode is 70 kV and the gas enters with an inlet velocity of 1m/s. The concentration distribution reveals that for an applied voltage, the dispersion of ultrafine particles (0.1 μm) is more as compared to micro-sized particles (1 μm and 10 μm). It is clearly evident from Fig. 15 that ultrafine particles are harder to collect as compared to micro-sized (accumulation mode and coarse mode) particles. The accumulative collection performance for these three different sized particles (0.1 μm, 1 μm and 10 μm) for an applied voltage of 70 kV is shown in Fig.16. Though there exists a notable increase in the percentage trapped for larger sized particles the improvement in accumulative collection performance is not too significant for sub-micron sized particles. In order to show the slight increase in the collection performance the accumulative collection performance of 100 nm (0.1 micron) sized particles is plotted for different electric potentials in Fig. 17.

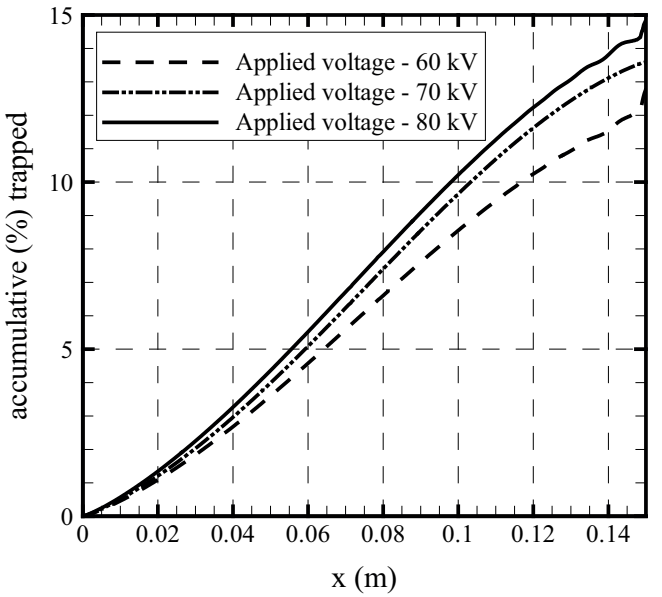

Figure 17: Accumulative collection performance for different electric potentials at the wire discharge electrode (particle size of 100 nm (0.1 micron))

4. CONCLUSIONS

In the present study, the behavior of a plate-plate and wire-plate ESP as a collection device for precharged particles in turbulent flow has been investigated. An Eulerian approach for modeling the particle concentration distribution in the presence of an inhomogeneous electric field is proposed. An attempt to obtain a complete solution for particle dynamics in both plate-plate and wire-plate ESPs is made. The present methodology provides a means of coupling the flow field, electric field, charging kinetics with the particle number concentration. The two representative cases considered for the investigation applies to the collection stage of a plate-plate (without corona discharge) and wire-plate ESP (with corona discharge). The effect of turbulent diffusivity on particle number concentration distribution is brought out clearly from the numerical analysis on plate-plate ESP. The effect of the particle size on the collection efficiency of a wire plate ESP is studied with due emphasize on the effect of applied voltage at the wire discharge electrode. The results obtained in the present paper, provides insight into the effects of non-uniform/inhomogeneous electric fields on the particle number concentration in the collection stage of a plate-plate and wire-plate ESP.

ACKNOWLEDGEMENTS

The financial support of OSEO France for conducting the present study is gratefully acknowledged.

Nomenclature

b_I	ionic mobility $=2 \times 10^{-4}$, [$m^2/V/s$]
C_c	Cunningham correction factor
$\overline{C_t}$	mean thermal speed of ions = 2.4×10^{22}, [m/s]
C_0	particle number concentration at inlet, [$1/m^3$]

C^{α}	particle number concentration of pollutant species, [1/m^3]
d_p	diameter of particles, m
$D\mu$	particle/Brownian diffusivity, [m^2/s]
D_t^{α}	turbulent diffusivity, [m^2/s]
e	electronic unit charge = 1.6×10^{-19}, [C]
E_j	electric field strength, [V/m]
i	coordinate index
j	coordinate index
k	turbulent kinetic energy, [m^2/s^2]
k_{β}	Boltzmann constant = 1.38×10^{-23}, [J/K]
n_{field}	number of charges by field charging
n_{diff}	number of charges by diffusion charging
p	pressure, [Pa]
q_p	charge of a single particle, [C]
Sc_t	turbulent Schmidt number
t	time, [s]
T	temperature, [K]
u_j	velocity, [m/s]
u_j^t	terminal velocity, [m/s]
w_e	electrical migration velocity, [m/s]
x_i, x_j	position, [m]
Greek symbols	
α	pollutant species
δ_{ij}	Kronecker delta
ε	turbulent dissipation rate, [m^2/s^3]
ε_0	dielectric permittivity of air = 8.859×10^{-12}, [As/V/m]
ϕ	electric potential, [V]
λ	mean free path of gas, [m]
μ	dynamic viscosity of gas, [kg/m/s]
μ_p	dielectric particle mobility, [As^2/kg]
μ_t	turbulent kinematic viscosity, [kg/m/s]
ρ	density, [kg/m^3]
$\rho_{el,I}$	ionic space charge density, [As/m^3 or C/ m^3]
$\rho_{el,p}$	particulate space charge density, [As/m^3 or C/ m^3]

REFERENCES

[1] A. Jaworek, A. Krupa, T. Czech, Modern electrostatic devices and methods for exhaust gas cleaning: A brief review, Journal of Electrostatics 65 (2007) 133–155.

[2] H. J. Schmid, On the modelling of the particle dynamics in electro-hydrodynamic flow field: II Influences of inhomogeneities on electrostatic precipitation, Powder Technology 135–136 (2003) 136–149.

[3] S. J. Park, S. S. Kim, Effects of particle space charge and turbulent diffusion on performance of plate-plate electrostatic precipitators, Journal of Electrostatics 45 (1998) 121–137.

[4] C. He, G. Ahmadi, Particle deposition in a nearly developed turbulent duct flow with electrophoresis, Journal of Aerosol Science 30 (1999) 739–758.

[5] H. J. Schmid, L. Vogel, On the modelling of the particle dynamics in electro-hydrodynamic flow-fields: I. Comparison of Eulerian and Lagrangian modelling approach, Powder Technology 135–136 (2003) 118–135.

[6] G. Skodras, S. P. Kaldis, D. Sofialidis, O. Faltsi, P. Grammelis, G. P. Sakerllaropoulos, Particulate removal via electrostatic precipitators, Fuel Processing Technology 87 (2006) 623–631.

[7] M. R. Talaie, Mathematical modeling of wire-duct single-stage electrostatic precipitators, Journal of Hazardous Materials B 124 (2005) 44–52.

[8] C. U. Bottner, The role of the space charge density in particulate processes in the example of the electrostatic precipitator, Powder Technology 135–136 (2003) 285–294.

[9] B. S. Choi, C. A. J. Fletcher, Turbulent particle dispersion in an electrostatic precipitator, Applied Mathematical Modelling 22 (1998) 1009–1021.

[10] G. Leonard, M. Mitchner, S. A. Self, Experimental study of the effect of turbulent diffusion on precipitator efficiency, Journal of Aerosol Science 13 (1982) 271–284.

[11] G. Leonard, M. Mitchner, S. A. Self, Particle transport in electrostatic precipitators, Atmospheric Environment 14 (1980) 1289–1299.

[12] G. Ahmadi, Modelling and computation of nanoparticles in fluid flows. Von Karman Lecture Series. RTO–AVT–VKI Lecture Series 2009.

[13] G. W. Penney, R. E. Matick, Potentials in D-C corona fields, Transactions of the American Institute of Electrical Engineers 79 (1960) 91–99.

[14] E. Lami, F. Mattachini, R. Sala, H. Vigl, A mathematical model of electrostatic field in wires-plate electrostatic precipitators, Journal of Electrostatics 39 (1997) 1–21.